Catalyst Evaluation and Kinetic Study for Ethylene Production

Angeliki A. Lemonidou* and Iacovos A. Vasalos

Department of Chemical Engineering and Chemical Process Engineering Research Institute, P.O. Box 19517, University City, 54006 Thessaloniki, Greece

Eugene J. Hirschberg and Ralph J. Bertolacini

Amoco Research Center, Naperville, Illinois 60566

The need to produce olefins via catalytic cracking has attracted increased attention in recent years. In this paper results are presented with catalysts composed of two or more of the following metal oxides: CaO, Al_2O_3, SrO, MgO, TiO_2, MnO_2, ZrO_2, and K_2O. A fixed bed reactor system was used to evaluate the catalysts with *n*-hexane as feedstock. The best results were obtained with calcium aluminate based catalysts. The higher olefins yields obtained with the new catalysts compared with α-Al_2O_3 are explained by the higher conversion obtained at the same process conditions. The kinetics of the pyrolysis of *n*-hexane was also studied. The overall decomposition reaction is first order both for thermal cracking and for cracking in the presence of catalyst $12CaO{\cdot}7Al_2O_3$. The kinetic parameters estimated in the presence of the catalyst are $k_{ow} = 4.57 \times 10^6$ cm^3/(g·s) and $E_w = 26\,130$ cal/mol.

Literature Review

The most commonly used method for manufacturing light olefins is introducing streams rich in paraffinic hydrocarbons, such as ethane, propane, and naphtha, into externally heated tubes. In this thermal decomposition process, the cracking reactions are controlled by varying the composition of the feed materials, the reaction temperature, and the residence time in the reaction tube.

This method has some drawbacks, such as the high temperature required for cracking reactions, the deposition of coke in the tubes, and especially low selectivity in ethylene and other desired products (Nowak and Gunschell, 1983).

To overcome these problems, a serious effort started a few years ago to introduce catalysts in the process. Various catalytic processes for the preparation of olefins have been reported, but these processes have not yet been applied commercially because of various difficulties.

Wrisberg et al. (1973) and Andersen et al. (1975) proposed as a catalyst a mixture of zirconium and hafnium oxides associated with active alumina to increase the mechanical strength. The main advantage of this type of catalyst is the minimization of the coke production, which was achieved by adding to the catalyst a small amount of alkali metals or alkaline-earth oxides, especially K_2O.

The oxides of zirconium and hafnium were used as carriers in the catalyst proposed by Colombos et al. (1978a,b). They used as an active compound MnO_2 on carrier ZrO_2 or HfO_2. The feedstock was atmospheric residue, and the ethylene yield was relatively good.

According to the studies of Pop et al. (1979), a bifunctional synthetic mordenite having the formula $(yH{\cdot}zM{\cdot}uNa)O{\cdot}Al_2O_3{\cdot}SiO_2$ (M = Cu, Ag, Co) was used, with very good yields of ethylene at relatively low temperatures. In this patent there is no mention of coke yields, perhaps high because of the type of catalyst used.

A different type of catalyst was proposed by Yegiazarov et al. (1978), consisting of In_2O_3 on pumice. The yield of ethylene was high and the coke deposition negligible. The high price of In_2O_3 is a discouraging factor for this approach. Adelson et al. (1979) suggested KVO_3 on pumice as a catalyst for the production of ethylene, with promising results.

Senes et al. (1972) proposed a catalyst with low porosity and containing at least one oxide of the metals of the group, formed by the rare earths and antimony, in small amounts in association with a mixture of refractory oxides with magnesium oxide and zirconium or aluminum oxide. The results were rather discouraging.

The most important research has been done at Toyo Engineering Corp. where Tomita et al. (1973, 1976) suggested a catalyst characterized by high ethylene yield and low coke deposition. The catalyst consists of refractory calcium aluminate with one oxide of the group of calcium, beryllium, magnesium, or strontium oxide. All the catalysts they proposed were of low porosity and surface area and of high crystallinity. The best results were obtained by a simple catalyst proposed by Kikuchi et al. (1985) with 51.46% CaO and 47.73% Al_2O_3. The crystal phase consists of a mixture of the aluminates $Ca_{12}Al_{14}O_{33}$ and $Ca_3Al_3O_6$. The yield in ethylene varies between 34 and 39 wt % depending on the temperature, pressure, steam-to-oil ratio, and contact time. The disadvantage of this process is the high yield of carbon dioxide.

In trying to assess the work of previous investigators, one quickly concludes that there is no limitation to the number or type of oxides proposed. However, the use of alumina oxide as a carrier or as an active component is common. There is also general agreement that the catalyst should be a mixture of at least two oxides, usually refractory.

Most of the catalysts disclosed have low porosity, high crushing strength, and very low surface area, except for the mordenite-type catalysts.

There is generally limited literature information regarding the kinetic mechanism with these catalysts. Tomita et al. (1973) suggest that alkaline-earth metal oxides control the dehydrogenation reaction of the feed hydrocarbons to prevent carbon deposition. They also suggest that aluminum oxide promotes the reaction between hydrocarbons and steam.

Based in the literature review, it is therefore concluded that the process of cracking hydrocarbons to produce lower olefins in the presence of catalysts is still under development and much work remains to be done.

Experimental Section

Catalyst Preparation and Characterization. On the basis of the literature search, several catalyst samples were prepared using a mixture of at least two metal oxides. The aim was to produce an identifiable crystal structure. It was realized that mechanical properties like crushing

0888-5885/89/2628-0524$01.50/0

Table I. Catalyst Composition and Properties

catalyst	CaO	Al_2O_3	SrO	MgO	In_2O_3	TiO_2	MnO_2	ZrO_2	K_2O	pumice	calcining temp, °C	surface area, m^2/g	crystal structure
101	1	1									1300	0.1	$CaAl_2O_4$
102	3	1									1300	0.31[a]	$Ca_3Al_2O_6$
103	12	7									1300	0.24[a]	$Ca_{12}Al_{14}O_{33}$·$Ca_3Al_2O_6$
104	1	2									1300	0.3	$CaAl_4O_7$
105	1	6									1300	2.1	$CaAl_{12}O_{19}$
201	3	2	1								1300	0.1	$Ca_3Al_2O_6$
202	3	2	3								1300	0.7	$Ca_3Al_2O_6$
203	12	8	1								1300	0.1	$Ca_{12}Al_{14}O_{33}$·$Ca_3Al_2O_6$
204		1	1								1300	0.4	$SrAl_2O_4$·$Sr_3Al_2O_6$
301		1		1							1300	1.9	$MgAlO_4$
401					1					13[b]	800	7.2	In_2O_3
402	1				1						800	4.3	$CaInO_4$·In_2O_3
501				1		7			1		950	3.5	K_2MgTiO_{16}
502						1	1				950	0.6	TiO_2
503							1	1			650	4.3	ZrO_2

[a] Multipoint BET surface area. [b] In grams/mole of oxide.

Table II. Correlation between Calcination Temperature, Surface Area, and Coke Production

catalyst	crystal structure	calcination temp, °C	surface area, m^2/g	coke yield, wt % on feed
1300	$Ca_{12}Al_{14}O_{33}$· $Ca_3Al_2O_6$	1300	3.05	0.11
1100	$Ca_{12}Al_{14}O_{33}$· $Ca_3Al_2O_6$	1100	5.20	0.60
850	$CaO·Al_2O_3$	850	20.00	4.50
600	$CaCO_3$	600	100.00	4.85

strength should be considered at a later stage.

The procedure for preparing the catalyst samples was as follows: A fixed quantity of each oxide (in nitrate or carbonate form) was placed in a ball mill for 1 h. Distilled water with a small amount of an organic binding agent was then added to the mixture. The amount of water is an important factor in determining the plasticity of the sample. After the sample is extruded to the desired size, the catalyst is first dried and then heated to 600 °C to convert nitrates to oxides. The crystal structure is then formed by calcination for 24 h at a high temperature. The calcination temperature is selected from the phase diagram, while the calcination time is chosen high enough to ensure the formation of the crystal structure.

Standard analytical techniques were used for the characterization of all catalyst samples prepared. To identify the crystal structure formed after the calcination procedure, the samples were tested in a Miniflex-Rigaku diffractometer with monochromatized Cu $K\alpha_1$ radiation and a Ni filter. Crystal phases identified are shown in Table I.

Measurements of the surface area of the samples using the BET single-point technique are also shown in Table I.

A second series of catalysts containing the same metal oxides was prepared by calcination at different temperatures. The properties of these catalysts are listed in Table II.

All catalysts were compared with α-Al_2O_3 prepared from γ-Al_2O_3 by calcination at 1350 °C for 17 h.

Experimental Apparatus and Testing Procedure. A schematic diagram of the experimental unit is shown in Figure 1. The unit is conveniently divided into three sections: feed preparation, reactor section and liquid collection, gas analysis.

n-Hexane was used as the standard feed for all tests. The feed is picked up with nitrogen, and it is then introduced into the upper reactor section where it is mixed with steam. The water, after measuring its flow, is vaporized in a furnace, and it is then heated to the desired temperature with a wall heater.

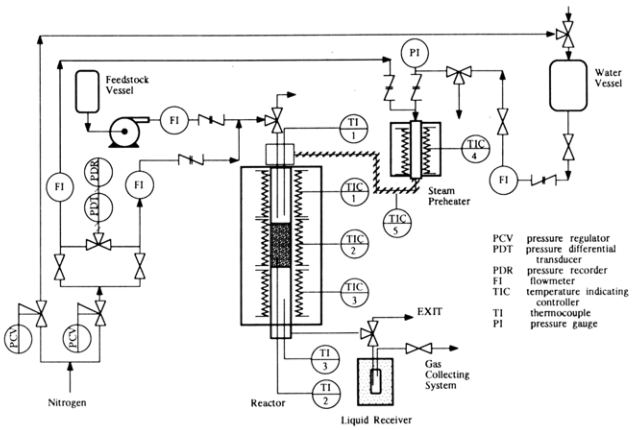

Figure 1. Schematic diagram of the experimental unit for the evaluation of catalysts.

A stainless steel reactor (1.25-cm i.d.) was used. A stainless steel screen located in the center of the reactor holds the catalyst. A three-zone furnace was used to control the reactor temperature, which was monitored at three locations. The temperature within the reactor was measured by three Chromel–Alumel thermocouples located in the feed inlet, in the catalyst bed, and in the lower part of the reactor.

The products at the reactor exit are first cooled in an ice-cooled liquid receiver where the steam and heavy hydrocarbons are condensed. The gases then flow to a gas-collecting system where the volume is measured by water displacement. The gases are analyzed in two gas chromatographs. A Varian 3700 with a thermal conductivity detector and a Carbosphere column is used to analyze for H_2, N_2, CH_4, CO, and CO_2.

Hydrocarbons (paraffins and olefins with up to six carbon atoms) are analyzed in a HP 5710A gas chromatograph equipped with a FID detector and a Porapak Q column. *n*-Hexane unreacted is partly collected as liquid in the receiver with water and partly collected as gas in the gas product collecting system.

Experimental Conditions. All catalysts were evaluated at the following conditions: *n*-hexane flow rate, 0.465–0.498 g/min; steam flow rate, 1.7 g/min; nitrogen flow rate, 30–32 mL/min; reaction temperature, 782–786 °C; space velocity, 9–10 h^{-1}; run time, 75 s; catalyst weight, 3 g; and catalyst diameter, 0.159 cm.

An effort was made to maintain the temperature constant during the runs. This was attained with the three-zone furnace equipped with temperature-indicating controllers, PID. Plug flow conditions were tested with a suitable tracer response analysis.

A series of runs were carried out to establish the kinetic parameters for the decomposition of *n*-hexane to lighter products. Feed flow rate, steam flow rate, and reaction temperature were varied within the limits of the experimental unit. The range of the experimental conditions was as follows: *n*-hexane flow rate, 0.23–0.86 g/min; steam flow rate, 0.92–3.3 g/min; nitrogen flow rate, 30 mL/min; reaction temperature, 730–780 °C; space velocity, 4.6–17.2 h^{-1}; run time, 75 s; catalyst weight, 3 g; and catalyst diameter, 0.159 cm.

The reaction temperature mentioned above refers to the temperature measured during the reaction in the catalyst zone.

Composition Effects

Catalyst samples with different chemical compositions were tested under the same experimental conditions. The results of this testing are reported in Table III. Evaluation of the samples was based not only on the yield of the desired products (C_2H_4, C_3H_6) but also on the undesired products (CO, CO_2, CH_4). Two selectivity ratios were proposed, one expressing the ratio of C_2H_4 and C_3H_6 yields to CO_2 and CO yields and the other expressing the ratio of C_2H_4 and C_3H_6 yields to CO_2, CO, and CH_4 yields. The higher the two selectivity ratios, the more suitable the catalyst for the process.

The main conclusions from these results are as follows:

1. Contrary to what has been reported in the literature by Colombos et al. (1978a,b), the selectivity ratios of the oxides of Mn, Ti, and Zr are low. It should be mentioned that the MnO_2·TiO_2 catalyst shows a moderate activity, whereas the MnO_2·ZrO_2 sample shows a low activity, mainly due to the high carbon oxides yield.

2. In_2O_3 on pumice shows moderate selectivity in promoting the desired products. The lower selectivity of this catalyst compared with the one reported by Yegiazarov et al. (1978) is probably due to the higher space velocity used in this study, 9 h^{-1}.

3. The results of combinations of metal oxides of CaO and/or Al_2O_3 with SrO are not successful because of the low selectivity ratios. The cause of this low selectivity is the relatively high carbon oxides yield especially with samples 3CaO·SrO·2Al_2O_3 and SrO·Al_2O_3.

4. The best results were obtained with catalysts containing CaO and Al_2O_3, depending on the molar proportions of the oxides. X-ray diffraction analysis of these samples indicated that the formation of a certain crystal phase depends mainly on the molar proportions of the component oxides. Selectivity ratios vary with the molar proportions of CaO and Al_2O_3. The mixture of CaO and Al_2O_3 at a molar ratio of 12:7 shows the highest selectivity ratios of all catalyst samples prepared. Kikuchi et al. (1985) proposed this type of catalyst, 12CaO·7Al_2O_3, for the production of ethylene, with very promising results. The X-ray diffraction pattern of this sample shows the formation of two crystal phases, one of $Ca_{12}Al_{14}O_{33}$ as a major component and the other of $Ca_3Al_2O_6$ as a minor component. It was difficult to reproduce samples with pure $Ca_{12}Al_{14}O_{33}$ crystal phase. The presence of the two phases has also been reported by Kikuchi et al. (1985).

α-Alumina samples tested under the same experimental conditions showed relatively low selectivity ratios mainly due to the low ethylene and propylene yields. Cracking of *n*-hexane in an empty reactor shows low selectivity due to the lower olefins yields. It is worth noting that some catalyst samples have lower selectivity than the relatively "inert" α-Al_2O_3 and even lower than that of thermal cracking (empty reactor) because of the high carbon oxide yields.

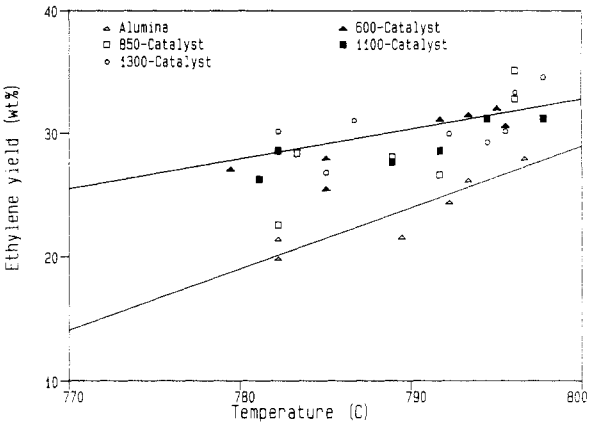

Figure 2. Ethylene yield in the presence of catalyst samples, calcined at different temperatures and in the presence of α-alumina.

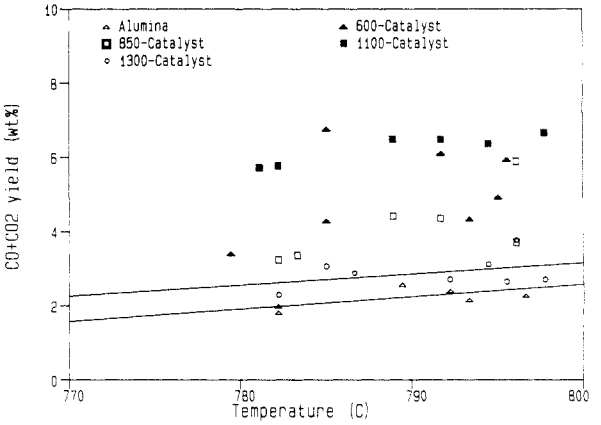

Figure 3. Carbon oxides yield in the presence of catalyst samples calcined at different temperatures and in the presence of α-alumina.

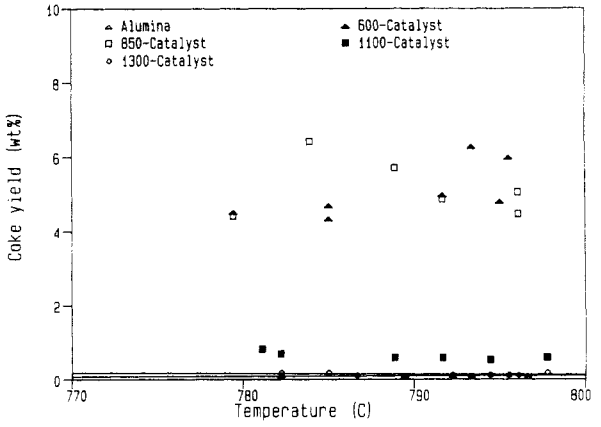

Figure 4. Coke yield in the presence of catalyst samples, calcined at different temperatures and in the presence of α-alumina.

Calcium Aluminate Based Catalysts

Realizing that a new catalytic process for producing ethylene should minimize the formation of coke on catalyst, a catalyst composed of 44 wt % CaO and 56 wt % Al_2O_3 was calcined at the following temperatures: 600, 850, 1100, and 1300 °C. Testing was carried out at the conditions reported in the previous section.

A comparison of the ethylene, CO_2 + CO, and coke yields for the four different calcination temperatures is

Table III. Selectivity Ratios of Various Oxides

catalyst composition	C_2H_4, wt %	C_3H_6, wt %	CH_4, wt %	CO + CO_2, wt %	C_2H_4 + C_3H_6/ CO + CO_2	C_2H_4 + C_3H_6/ CO + CO_2 + CH_4	n-C_6 mass balance
$CaO{\cdot}Al_2O_3$	34.7	18.6	6.4	2.7	19.9	5.8	94.3
$12CaO{\cdot}7Al_2O_3$	34.8	19.0	6.0	1.7	31.6	6.9	94.2
$CaO{\cdot}2Al_2O_3$	33.3	18.9	6.2	1.9	26.3	6.3	95.7
$CaO{\cdot}6Al_2O_3$	32.7	15.6	4.5	4.2	11.2	5.5	92.1
$3CaO{\cdot}SrO{\cdot}2Al_2O_3$	30.3	17.8	5.2	2.8	16.7	5.9	97.3
$3CaO{\cdot}3SrO{\cdot}2Al_2O_3$	31.4	13.6	5.3	11.4	3.9	2.6	94.8
$12CaO{\cdot}SrO{\cdot}8Al_2O_3$	33.6	16.8	5.1	3.4	14.8	5.9	95.7
$SrO{\cdot}Al_2O_3$	29.8	14.3	5.6	6.4	6.9	3.6	92.3
$MgO{\cdot}Al_2O_3$	32.7	17.3	6.1	2.3	21.7	5.9	97.2
In_2O_3·pumice	31.5	15.8	5.9	1.8	26.5	6.0	96.7
$CaO{\cdot}In_2O_3$	32.0	16.7	5.3	10.7	4.5	3.0	97.7
$K_2O{\cdot}MgO{\cdot}7TiO_2$	28.7	15.8	5.3	1.9	23.3	6.3	95.2
$MnO_2{\cdot}TiO_2$	30.0	15.9	5.1	1.9	23.6	6.4	96.2
$ZrO_2{\cdot}MnO_2$	30.3	17.2	5.5	4.4	10.7	4.7	92.3
α-Al_2O_3	22.2	13.5	5.9	2.1	17.3	4.5	96.9
empty reactor	16.9	10.8	4.4	2.0	13.7	4.3	97.5

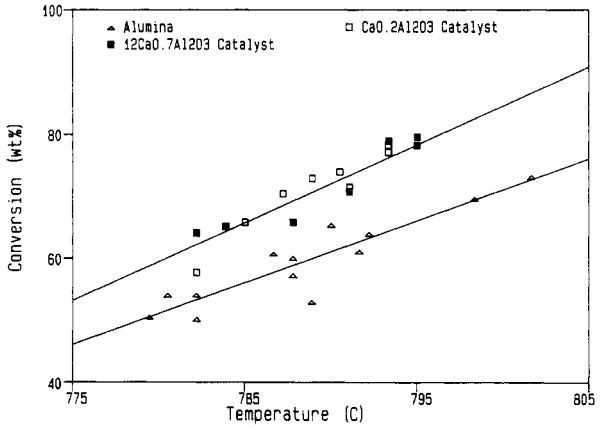

Figure 5. Effect of temperature on the n-hexane conversion in the presence of α-alumina and calcium aluminate catalysts.

shown in Figures 2–4. For comparison purposes, the results are also shown for α-Al_2O_3. In the preparation of the sample of α-Al_2O_3, an effort was made to reproduce a solid sample with the same pellet size and surface area as the sample of CaO/Al_2O_3 calcined at 1300 °C. It is not claimed, with this work, that α-Al_2O_3 is completely inactive. Adelson et al. (1979) proved that α-alumina and even quartz show some catalytic action compared with an empty reactor.

From a careful study of Figures 2–4, the following conclusions can be drawn:

1. The ethylene yield (Figure 2) with CaO/Al_2O_3 is higher than with α-Al_2O_3. However, there is no discernible difference between samples calcined at different temperatures.

2. Yields of CO_2 and CO are considerably lower for samples calcined at 1300 °C (Figure 3).

3. High calcination temperature leads to a substantial reduction in coke yield. As shown in Figure 4, catalysts calcined at 600 and 850 °C produce 4–6 wt % coke on fresh feed, while samples calcined at 1100 and 1300 °C produce 0.5–0.9 and 0.1–0.2 wt % coke, respectively.

X-ray diffraction clearly showed the absence of crystal structures at low calcining temperatures. It is believed that the low surface area of samples calcined at high temperatures is the primary reason for the low coke yield (Table II). Therefore, it is essential to calcine the catalyst samples at high temperatures so as to minimize the coke production.

The need to continue the evaluation of calcium aluminate based catalysts with samples of specific geometry necessitated the preparation of larger batches of catalyst

Table IV. Properties of Catalysts

sample	9034-168A	9034-170A
chem composition	$12CaO{\cdot}7Al_2O_3$	$CaO{\cdot}2Al_2O_3$
calcination temp, °C	1200	1200
calcination time, h	24	24
particle diameter, cm	0.159	0.159
surface area, m^2/g	2.08	4.45
XRD pattern	$Ca_{12}Al_{14}O_{33}{\cdot}Ca_3Al_2O_6$	$CaAl_4O_6$

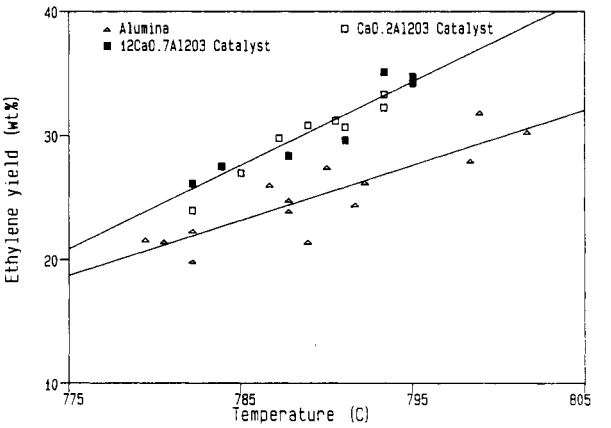

Figure 6. Effect of temperature on ethylene yield in the presence of α-alumina and calcium aluminate catalysts.

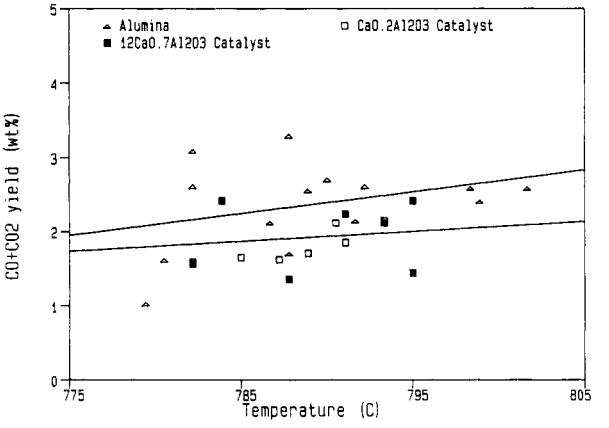

Figure 7. Effect of temperature on carbon oxides yield in the presence of α-alumina and calcium aluminate catalysts.

at Amoco Research Center. The properties of catalysts prepared in this manner are reported in Table IV.

The conversion of n-hexane and the yields of ethylene and carbon oxides are shown in Figures 5, 6, and 7, correspondingly. X-ray diffraction confirmed the existence of $Ca_3Al_2O_6$ and $Ca_{12}Al_{17}O_{33}$ in sample 9034-168A. The

Table V. Effect of Hydrogen Treatment on $12CaO \cdot 7Al_2O_3$ Catalyst Performance

type of catalyst	untreated	treated with H_2
test conditions		
temp, °C	780	780
feed flow rate, mL/min	0.68	0.68
H_2O flow rate, mL/min	1.7	1.7
catalyst wt, g	3	3
feed conversn, wt %	50.76	40.24
product yields, wt % (on feed)		
H_2	0.58	0.55
CH_4	5.10	4.28
C_2H_6	1.16	0.89
C_2H_4	21.51	17.08
C_3H_8	0.38	0.25
C_3H_6	13.06	10.24
C_4H_8	7.21	5.56
C_4H_6	1.41	1.11
CO_2	1.14	0.83
CO	0.18	0.27
feed recovery, wt %	96.70	97.80

results shown in Figures 5–7 confirmed again the higher yield of ethylene with these catalysts compared with α-Al_2O_3.

To explain the increase in the feedstock conversion occurring in the presence of calcium aluminate, a catalyst sample was treated with hydrogen in a thermal gravimetric balance (Du Pont Series 99 thermal analyzer). The catalyst weight was reduced by 1.5% between 780 and 800 °C.

The reduced catalyst sample was subsequently tested at 780 °C. The results of testing catalyst samples treated and untreated with hydrogen are reported in Table V. A decrease in the feedstock conversion was observed when the catalyst was treated with hydrogen.

It is therefore believed that the catalytic action is due to the presence of active oxygen of the calcium aluminate catalyst. This oxygen is leaving the system in the form of water after the catalyst was treated with hydrogen.

The presence of active oxygen in calcium aluminates was identified and studied in detail by Imlach et al. (1971) and by Brisi and Lucco-Borlera (1983). This active oxygen promotes nonselectively all the cracking reactions, as is concluded from the same selectivity ratios obtained in thermal and catalytic cracking. This action of oxygen was confirmed by many research groups involved in methane oxidative coupling (Ito et al., 1985; Keller and Bhasin, 1982; Hinsen and Baerns, 1983). They claim that oxygen in the catalysts (alkaline, or alkaline-earth oxides with very low surface area) promotes the formation of methyl radicals at the catalyst surface and hence the overall cracking reactions of hydrocarbons in the gas phase.

Pyrolysis Model

A simplified first-order reaction pyrolysis model was used to fit the kinetic data. It was found that the reactor behaved as an integral nonisothermal reactor, and for calculation purposes it was divided into three zones as indicated in Figure 8. The following assumptions were made:

1. Each reactor zone behaves in a plug flow mode.
2. For estimation purposes, each zone can be treated at constant temperature.
3. Because of the high dilution of steam, there is no appreciable volume expansions.

Based on the above assumptions, the following equations describe the conversion of n-hexane for each reactor zone:

$$(-r_A)_i \, dV_i = F_{A0,i} \, dX_{Ai} \qquad i = 1\text{–}3 \tag{1}$$

$$(-r_A)_i = K(T_i) C_{Ai} \tag{2}$$

$$1 - X_A = (1 - X_{A1})(1 - X_{A2})(1 - X_{A3}) \tag{3}$$

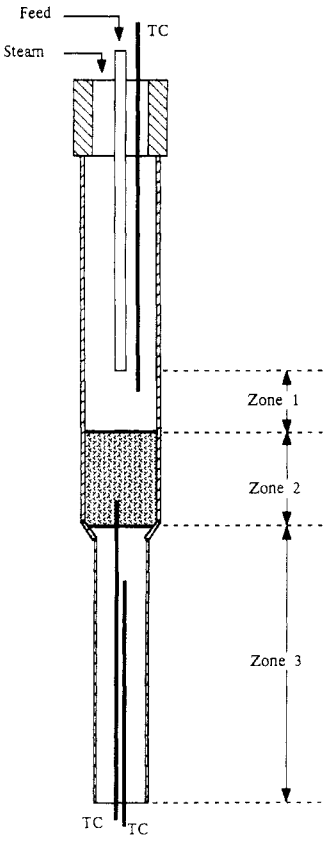

Figure 8. Reactor configuration.

where $(-r_A)_i$ is the rate of disappearance of n-hexane, $K(T_i)$ is the rate constant at temperature T_i, C_{Ai} is the n-hexane concentration, $F_{A0,i}$ is the molar flow rate of the reactant in the inlet of each reactor zone, V_i is the volume of each reactor zone, X_{Ai} is the n-hexane conversion at each reactor zone, and X_A is the total conversion at the exit of the reactor.

In reactor sections where no solids are present, the rate constant is equal to the thermal cracking rate constant K_v. For the middle reaction section where solids are present, we assume that two parallel paths of cracking reactions occur: in the bulk between the particles and on the particle surface.

The design equations for this case are the same as (1) and (2), but the rate constant is equal to

$$K = K_v \epsilon + K_w (1 - \epsilon) \rho_p \tag{4}$$

where K_v and K_w are the rate constants for thermal and catalytic reactions, respectively, ϵ is the void fraction of the catalytic bed, and ρ_p is the particle density.

The assumption of the two parallel paths in describing the decomposition reactions in the presence of particles is valid because there are no selectivity differences between cracking in the presence of particles (α-alumina, $12CaO \cdot 7Al_2O_3$ catalyst) and thermal cracking (empty reactor). Product selectivity is defined as grams of each product per 100 g of n-hexane converted (Figures 9–11).

By use of (1)–(3) and the experimental conversion for kinetic runs in an empty reactor, the Arrhenius parameters of the overall thermal decomposition rate of n-hexane were obtained by using the algorithm of Levenberg–Marquadt. The estimated values of the two parameters K_{ov} and E_v for thermal cracking runs were used also for the estimation of the values of the kinetic parameters describing the phenomenon in the presence of solids (alumina, catalyst). The following numerical values were obtained:

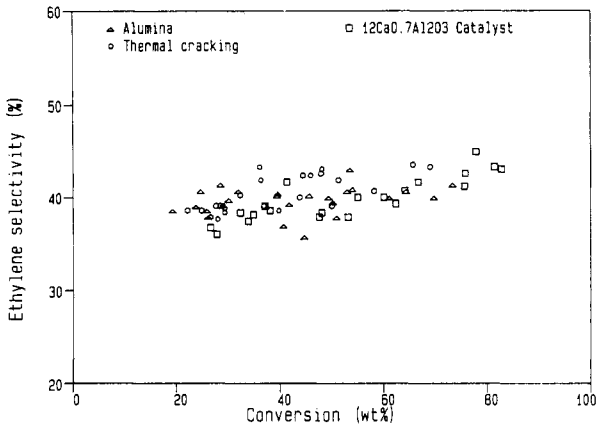

Figure 9. Ethylene selectivity as a function of feed conversion.

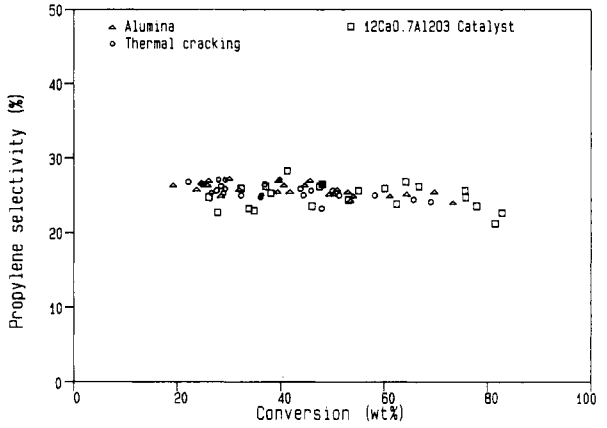

Figure 10. Propylene selectivity as a function of feed conversion.

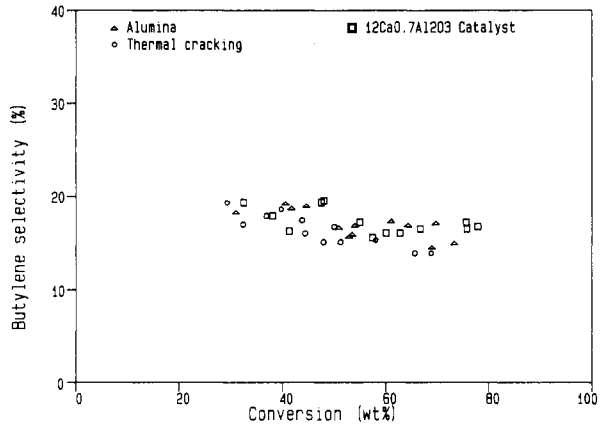

Figure 11. Butylene selectivity as a function of feed conversion.

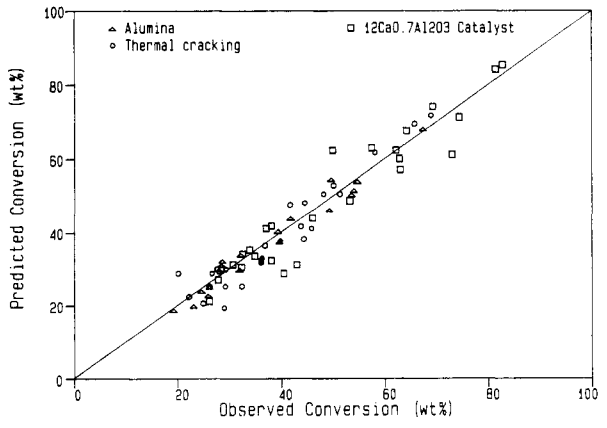

Figure 12. Relationship between the predicted feed conversion by the first-order kinetic model and the experimental conversion.

cracking	frequency factor, $cm^3/(g \cdot s)$	activation energy, cal/mol
thermal	0.206×10^9 (s^{-1})	35 680
alumina	2.16×10^8	36 500
catalytic	4.6×10^6	26 100

The results of the application of the Levenberg–Marquadt algorithm in all the kinetic runs are reported in the supplementary material. The adequacy of the first-order reaction model proposed is shown in Figure 12. It is evident that the calculated *n*-hexane conversion by the simplified kinetic model proposed for thermal, alumina, and catalytic cracking is in good agreement with the experimental values.

To our knowledge, there are no literature data concerning the values of the *n*-hexane kinetic parameters in the presence of α-Al_2O_3 and $12CaO \cdot 7Al_2O_3$ catalyst. The estimated values of the thermal cracking kinetic parameters are somewhat lower than those reported in the literature for the decomposition of *n*-hexane (Zdonik et al., 1970; Illes et al., 1973; Ebert et al., 1983). The experimental data used for the estimation of the kinetic parameters cover a wide range of conversion. As it is known, the reaction rate constant decreases with increasing conversion. This is due to the self-inhibition effect as described by Leathard and Purnell (1970). For the data collected at high conversion, the self-inhibition effect has to be taken into account. The dependence of the rate constant on conversion is expressed by

$$K = \frac{K_z}{1 + \alpha X_\alpha}$$

where K_z is the rate constant at very low conversions (<10%), known as zero conversion, and α is the inhibition coefficient.

Application of the Levenberg–Marquadt algorithm to the results of the thermal cracking runs, taking into account the inhibition effect, improves the estimation of the kinetic constants K_{oz} and E_z.

The estimated values of K_{oz} and E_z and the estimation of the inhibition coefficient are $K_{oz} = 0.43 \times 10^{12}$ s^{-1}, $E_z = 51\,000$ cal/mol, and $\alpha = 3.15$.

The calculated kinetic parameters accounting for the self-inhibition effect of the products are very similar to those reported in the literature (Zdonik et al., 1970; Illes et al., 1973; Ebert et al., 1983). The inhibition coefficient was found lower than the one calculated by Murata and Saito (1975) for the cracking of *n*-hexane. The main reason for this may be attributed to the higher dilution ratio (Illes et al., 1973) used in our study.

The inhibition effect affects the estimation of the kinetic parameters for the cracking in the presence of α-alumina and catalyst $12CaO \cdot 7Al_2O_3$. It was assumed that the inhibition coefficient has the same value with that estimated for thermal cracking because of the same type of feedstock and similar dilution ratio used.

The calculated kinetic parameters are

	K_{oz}, $cm^3/(g \cdot s)$	E_z, cal/mol
α-Al_2O_3	3.43×10^8	36 460
$12CaO \cdot 7Al_2O_3$ catalyst	8.95×10^6	26 350

The differences between the experimental conversion and that calculated by the inhibition model are very small, as is shown in Figure 13.

Conclusions

The best results were obtained with calcium aluminate catalysts at a CaO-to-Al_2O_3 molar ratio of 12:7 and a

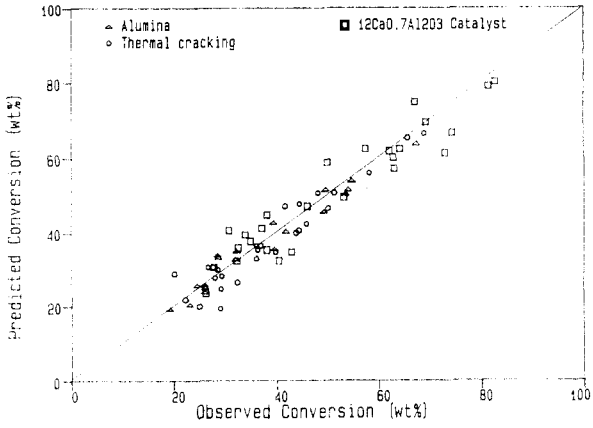

Figure 13. Relationship between the predicted feed conversion and the experimental for the model taking into account the inhibition effect.

calcination temperature of 1300 °C.

Samples calcined at low temperature favor the formation of coke. Therefore, high calcination temperature is necessary to minimize coke production.

Comparison of product yields in the presence of α-Al_2O_3 with those of calcium aluminate catalysts leads to higher olefins yield in the presence of $12CaO{\cdot}7Al_2O_3$, mainly due to the higher degree of hexane conversion.

No selectivity differences exist between calcium aluminate catalyst and α-Al_2O_3 at the same conversion level. The overall thermal decomposition of n-C_6H_{14} is well described by the first-order reaction model. In the presence of α-alumina and of catalyst $12CaO{\cdot}7Al_2O_3$, the overall cracking reactions are also described by first-order reaction models.

The inhibition effect of the products on the overall kinetic rate constant was also studied, and it was found to be significant for the thermal cracking and for the cracking in the presence of α-alumina and $12CaO{\cdot}7Al_2O_3$ catalyst.

Acknowledgment

A. A. Lemonidou and I. A. Vasalos thank the Secretariat of Research and Technology for the financial support of this research.

Nomenclature

$(-r_A)_i$ = rate of disappearance, mol/(s·cm^3)
C_{Ai} = reactant concentration, mol/cm^3
$F_{A0,i}$ = initial molar flow of reactant in the inlet of each reactor zone, mol/s
V_i = volume of each reactor zone, cm^3
X_{Ai} = conversion at the end of each zone, wt %
X_A = conversion at the exit of the reactor, wt %
K = rate constant, s^{-1}
K_v = thermal cracking reaction rate constant, s^{-1}
K_w = catalytic cracking reaction rate constant, cm^3/(g·s)
K_{ov} = frequency factor for thermal decomposition, s^{-1}
K_{ow} = frequency factor for catalytic decomposition, cm^3/(g·s)
K_{oz} = frequency factor for zero conversion, s^{-1}
E_v = activation energy for thermal decomposition, cal/mol
E_w = activation energy for catalytic decomposition, cal/mol
E_z = activation energy for zero conversion, cal/mol

Greek Symbols

ϵ = void fraction of the catalytic bed
ρ_p = particle density, g/cm^3
α = inhibition coefficient

Supplementary Material Available: Tables I–III reporting the estimated values of conversions for each reactor zone, the residuals of each run, and the residual sum of squares for the thermal cracking kinetic runs and for kinetic runs in the presence of α-Al_2O_3 and $12CaO{\cdot}7Al_2O_3$ catalysts (3 pages). Ordering information is given on any current masthead page.

Literature Cited

Adelson, S. V.; Vorontsova, T. A.; Melnikova, S. A. *Neftekhimiya* **1979**, *19*, 577.
Andersen, K. J.; Fischer, F.; Rostrup-Nielsen, J.; Wrisberg, J. US Patent 3,872,179, 1975.
Brisi, C.; Lucco-Borlera, M. *Cemento* **1983**, *3*, 155.
Colombos, A. J.; McNeice, D.; Wood, D. C. US Patent 4,087,350, 1978a.
Colombos, A. J.; McNeice, D.; Wood, D. C. US Patent 4,111,793, 1978b.
Ebert, K. H.; Ederer, H. J.; Isbarn, G. *Int. J. Chem. Kinet.* **1983**, *15*, 475.
Hinsen, W.; Baerns, M. *Chem.-Ztg.* **1983**, *107*, 223.
Illes, V.; Welther, K.; Pleszkats, I. *Acta Chim. Hung.* **1973**, *78*, 357.
Imlach, J. A.; Dent Glasser, L. S.; Glasser, F. P. *Cem. Concr. Res.* **1971**, *1*, 57.
Ito, T.; Wang, J.-X.; Lin, C.-H.; Lunsford, J. H. *J. Am. Chem. Soc.* **1985**, *107*, 5062.
Keller, G. E.; Bhasin, M. M. *J. Catal.* **1982**, *73*, 9.
Kikuchi, K.; Tomita, T.; Sakamoto, T.; Ishida, K. *Chem. Eng. Prog.* **1985**, *81* (No. 6), 54.
Leathard, D. A.; Purnell, J. H. *Ann. Rev. Phys. Chem.* **1970**, *21*, 197.
Murata, M.; Saito, S. *J. Chem. Eng. Jpn.* **1975**, *8*, 1, 39.
Nowak, S.; Gunschell, H. Pyrolysis of Petroleum Liquids: Naphthas to Crude. In *Pyrolysis: Theory and Industrial Practice*; Albright, L. F., Crynes, B. L., Concoran, W. H., Eds.; Academic: New York, 1983; p 319.
Pop, G.; Ivanus, G.; Boteanu, S.; Tomi, P.; Pop, E. US Patent 4, 172,816, 1979.
Senes, M.; Lhonore, P.; Quibel, J. US Patent 3,644,557, 1972.
Tomita, T.; Kikuchi, K.; Sakamoto, T. US Patent 3,767,567, 1973.
Tomita, T.; Kikuchi, K.; Sakamoto, T. US Patent 3,969,542, 1976.
Wrisberg, J.; Andersen, K. J.; Mogensen, E. US Patent 3,725,495, 1973.
Yegiazarov, G. Iu.; Cherches, B. Kh.; Krutko, N. P.; Pauskin, I. M. *Neftekhimiya* **1978**, *18*, 237.
Zdonik, S. B.; Green, E. J.; Hallee, L. P. *Manufacturing Ethylene*; The Petroleum Publishing Co.: Tulsa, OK, 1970; p 27.

Received for review July 27, 1987
Revised manuscript received March 4, 1988
Accepted January 13, 1989